Chemical Science

ROYAL SOCIETY OF CHEMISTRY

EDGE ARTICLE

View Article Online
View Journal | View Issue

Cite this: *Chem. Sci.*, 2025, **16**, 8800

All publication charges for this article have been paid for by the Royal Society of Chemistry

Received 1st February 2025
Accepted 10th April 2025

DOI: 10.1039/d5sc00851d

rsc.li/chemical-science

Accelerated click reactions using boronic acids for heterocyclic synthesis in microdroplets†

Jyotirmoy Ghosh and R. Graham Cooks *

Click chemistry is important for its simplicity and versatility, however, condensation-based click reactions are limited by the general requirement of high temperatures and catalysts. Here, we report accelerated click reactions using boronic acids in microdroplets under ambient conditions without a catalyst. The reaction between 2-formyl phenylboronic acid (2-FPBA) and substituted amines leads to the formation of multi-step click products, including iminoboronates, boroxines, thiazolidines, and diazaborines, depending on the selected amine. The reactions occur during microdroplet flight and are three orders of magnitude faster than the corresponding bulk reactions. MS and NMR spectral analysis confirmed the nature of the products. We suggest that the air–liquid interface of microdroplets serves both as a superacid and as a drying surface, facilitating dehydration by its superacidicity to access these products. We also demonstrate the application of these accelerated reactions as a late-stage functionalization (LSF) tool to access a range of antihistamine drug derivatives.

Introduction

Microdroplets are known to facilitate accelerated chemical reactions and this has implications for small-scale synthesis,[1–6] materials science,[7–11] drug discovery,[12–14] atmospheric chemistry,[15–18] and studies on the origin of life.[19–21] Reaction acceleration is associated with several factors, principally partial solvation[22,23] and the high interfacial electric field[10,24–27] with its constituent extreme pH gradient.[1,28,29] Less securely, confinement effects[30,31] and ordered molecular orientations[32,33] are also shown to contribute. A variety of chemical reactions in microdroplets are accelerated[19,29,34–39] without the need for a catalyst or high temperatures. Among these reactions, condensation[19] and click reactions[29] are of particular interest due to their implications in origin-of-life studies and for bioorthogonal chemistry.

The formation of iminoboronates upon reaction of amines with 2-formyl phenylboronic acid (2-FPBA) involves a condensation click reaction.[40–42] Iminoboronates are an emerging class of compounds that include imines positioned *ortho* to an aryl boronic acid, where a dative bond is formed between the imine nitrogen and the electron-deficient boron. Owing to this proximity effect, iminoboronates display significantly higher equilibrium constants and much-improved thermodynamic stability than other simple imines without a neighboring aryl boronic acid.[43] Iminoboronate chemistry has been applied in protein side-chain modification,[44] as a chiral derivatization protocol for determining the enantiopurity of chiral amines/amino acids,[45] in creating self-healing polymers,[42,46] and in studies of antibacterial activity.[47,48] In addition, the boronic acid functionality is capable of driving intermolecular condensation reactions to form the corresponding dimers and trimers. The dehydrated cyclic trimers of boronic acids, known as boroxines, are used as covalent organic framework (COF) building blocks[49–51] as reagents in Suzuki–Miyaura cross-coupling reactions,[52,53] in flame-retardant materials,[54] as optical components,[55] and in battery applications.[56] Iminoboronate chemistry is dynamic, proceeding down chemical pathways that depend upon the chosen amine: instances include the formation of

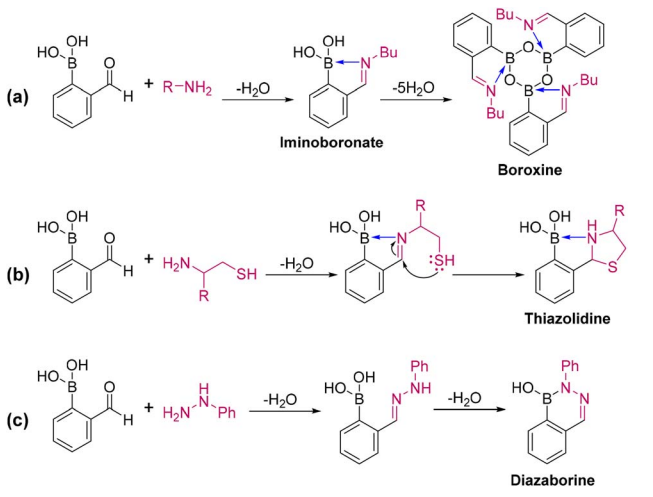

Scheme 1 Condensation-based click reactions of iminoboronates that lead to a variety of important chemical scaffolds.

Department of Chemistry, Purdue University, 560 Oval Drive, West Lafayette, IN 47907, USA. E-mail: cooks@purdue.edu

† Electronic supplementary information (ESI) available. See DOI: https://doi.org/10.1039/d5sc00851d

boroxines,[37] thiazolidines,[43,57] and diazaborines[58] (Scheme 1). Several drugs contain thiazolidine rings, especially the penicillins which are elaborated thiazolidines. Diazaborines are therapeutically important scaffolds that also have antibacterial activity.[47,48] Their mode of action involves inhibition of lipopolysaccharide biosynthesis in Gram-negative bacteria.[59] Most conventional methods for the synthesis of these dehydrated products require high temperatures/reflux conditions and long reaction times.[42] In sharp contrast, the present study shows accelerated syntheses of iminoboronate, boroxine, thiazolidine, and diazaborine under ambient conditions using microdroplets without any catalyst or elevated temperature. Furthermore, these accelerated reactions are shown in late-stage functionalization (LSF) to yield complex antihistamine drug derivatives.

Results and discussion

Reactions were performed by electrospraying mixtures of amines and 2-formyl phenylboronic acid (2-FPBA), each 10 mM in reagent grade acetonitrile (ACN) without additional drying except where indicated. Electrospraying involved the application of a positive DC potential of 1.5 kV using a nano-electrospray ionization (nESI) electrode with a 10 mm distance between the sprayer tip and MS inlet. See the ESI† for details of the experimental procedures.

Iminoboronate and boroxine formation in microdroplets

The formation of iminoboronate in microdroplets was carried out by spraying an equimolar mixture of butylamine and 2-FPBA in reagent grade acetonitrile solvent under ambient conditions. The first step in the reaction scheme (Fig. 1a) involves the formation of the corresponding iminoboronate, **3** by intramolecular condensation to form a (imine) covalent bond. The protonated iminoboronate product, $[\mathbf{3}+\mathbf{H}]^+$, and the corresponding cyclic boroxine, $[\mathbf{4}+\mathbf{H}]^+$, occur at *m*/*z* 206 and 562, respectively, in the nESI mass spectrum (Fig. 1b). Confirmation of the structure of **3** is found in its MS/MS (Fig. S1†) and by comparing the expected and experimental isotopic distributions (Fig. S2†). The proximal presence of electron-rich N to the electron-deficient B atom in the product results in a dative bond (blue arrow in **3**), a characteristic feature of iminoboronates. An intermolecular condensation product **5**, occurring at *m*/*z* 375, involves two iminoboronate molecules, as confirmed by the isotopic distribution (Fig. S3†). Interestingly, the reaction proceeded *via* further intermolecular condensation to form boroxine, a cyclic trimer of iminoboronate formed with the overall loss of five H_2O molecules. Reported syntheses of boroxines require reflux conditions to achieve dehydration.[42,49] Here, dehydration is favoured by the enhanced surface area, superacidity, and the 'dry' solution–air interface of microdroplets,[19,20] making boroxine the major product in the small-scale reaction occurring on the millisecond timescale, *i.e.*, during the flight of the droplets to the mass spectrometer. Note that the formation of a Lewis acid–base adduct with an adjacent N-donor also enhances the stability of the boroxine as observed in previous studies.[42,54,60] Structural confirmation of the boroxine product, **4** was achieved by MS/MS (Fig. 1c), and the fragmentation pathway is rationalized in Fig. S4.† In addition, a comparison of the calculated isotopic distribution with the experimental data (Fig. S5†) and NMR analysis (Fig. 2) confirms the identity of the product. Note that the reaction mixture was electrosprayed and collected without workup for NMR analysis. The NMR spectra were recorded after scaling up the reaction products by collecting the electrosprayed microdroplets (see the ESI†). The chemical shifts for the H atoms (H_a–H_d) adjacent to the N-center are used as a characteristic to identify the different products (Fig. 2). Peaks in the range 8.2–8.5 ppm are assigned to

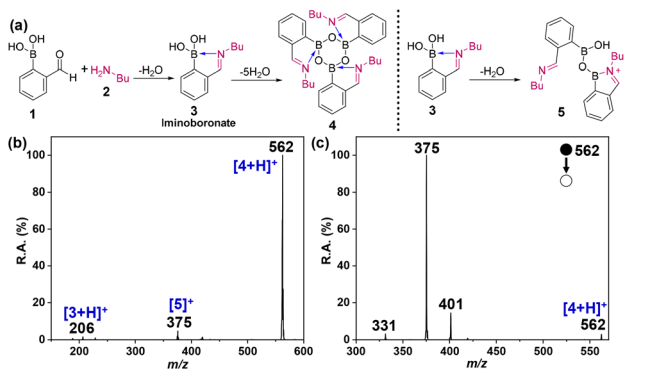

Fig. 1 (a) Reactions that form iminoboronate and boroxine in electrosprayed microdroplets. Reaction **3** → **5** involves dehydration of the dimer. (b) Positive mode nESI MS showing products of the reaction between butylamine and 2-FPBA in reagent grade ACN microdroplets. Structures for the labeled peaks are shown. (c) MS/MS spectrum of mass-selected boroxine product, $[\mathbf{4}+\mathbf{H}]^+$, *m*/*z* 562, recorded using collision-induced dissociation (CID). MS/MS spectra of other products are provided in the ESI.†

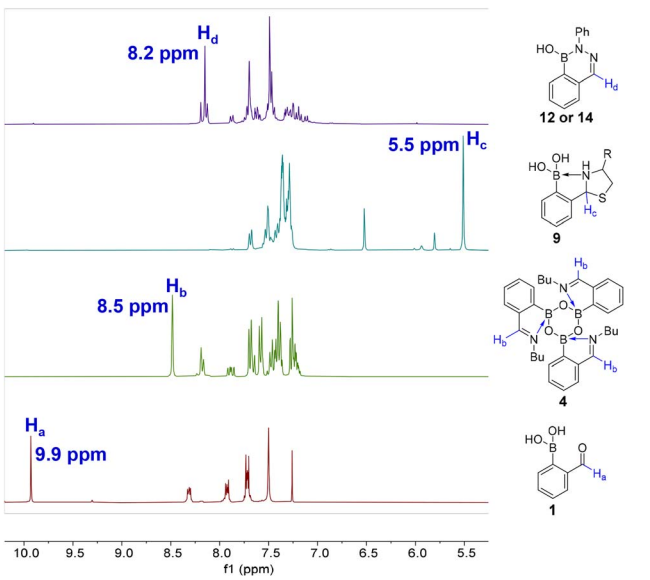

Fig. 2 ^{1}H NMR spectra (300 MHz, $CDCl_3$) showing the chemical shifts of the indicated protons (H_a–H_d) in different products obtained by reactions in microdroplets and analyzed without workup. The bottom spectrum is for standard 2-FPBA, **1**.

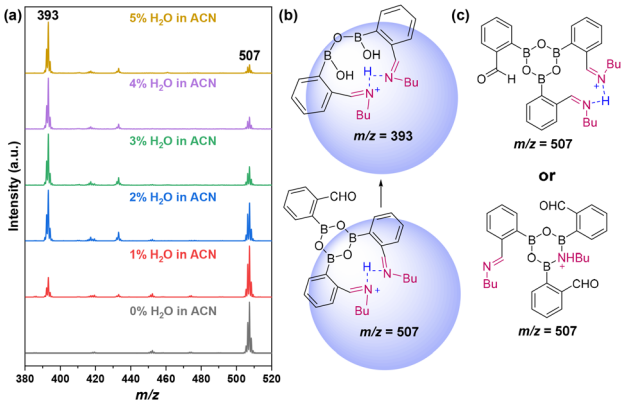

Fig. 3 (a) Positive mode nESI mass spectra of the products of reaction between butylamine and 2-FPBA using different ratios of H_2O:ACN in microdroplets. Here, water was added in specially dried ACN (see ESI,† Section 1.2). (b) Addition of water to the spray solvent gives the hydrolysis product, observed at *m*/*z* 393. (c) Isomeric chemical structures corresponding to *m*/*z* 507 are shown.

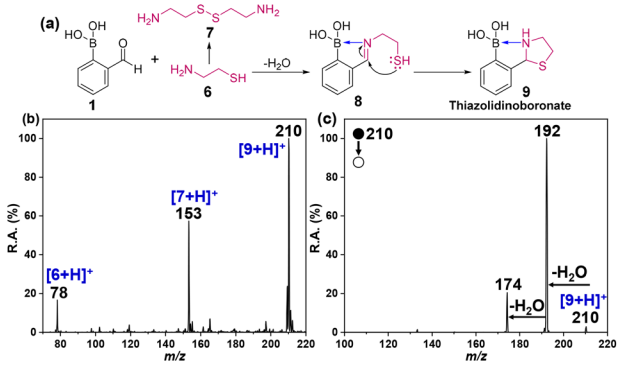

Fig. 4 (a) Formation of thiazolidinoboronate (**9**) *via* iminoboronate (**8**) in electropsrayed microdroplets. (b) Positive mode nESI mass spectrum showing the product of the reaction between cysteamine and 2-FPBA in ACN microdroplets. Structures are shown for the labeled peaks. (c) MS/MS spectrum of the mass-selected thiazolidinoboronate product, $[9+H]^+$, *m*/*z* 210, recorded using collision-induced dissociation (CID).

the H atoms (H_b and H_d) next to an imine bond in diazaborine[61] and boroxine,[42] whereas the equivalent H_c shows a peak at 5.5 ppm in thiazolidine, as observed previously.[62] The NMR spectrum of 2-FPBA was used as a control and it shows a completely different peak at 9.9 ppm for H_d.[63] The ^{11}B NMR spectrum was also recorded: it shows a peak at 15.14 ppm (Fig. S6†) and this together with the assigned ^1H NMR peaks (Fig. S7†) are characteristic signatures of the boroxine product, **4** as observed in a previous report.[42]

Solvent effects on the microdroplet reaction were also studied. First, an equimolar mixture of butylamine and 2-FPBA was electrosprayed using a specially dried ACN solvent (see ESI,† Section 1.2). Then, gradually, small amounts of water (v/v percent) were added to a set of otherwise identical reaction mixtures and mass spectra were recorded individually (Fig. 3a). In dry ACN, a peak at *m*/*z* 507 was observed, which corresponds to one of the two isomeric products (Fig. 3c). The formation of these products in the absence of water is ascribed to the preferential 'heads-down' orientation[32] of the positively charged reagents, the hydrophobic parts being anchored at the air–liquid interface of the microdroplets (Fig. 3b). The isomeric products are suggested to arise by the acid-catalysed mechanisms presented in Fig. S8.† The gradual addition of water to the spray solvent led to the formation of a hydrolyzed product (*m*/*z* 393) from the anchored species.

Thizaolidine complex formation in microdroplets

Following the successful synthesis of iminoboronate by click chemistry in microdroplets, we explored related chemical reactions involving iminoboronates. Iminoboronates can be repurposed to form thermodynamically stable heterocycles, notably the thiazolidine ring.[43,57] This reaction involves a nucleophilic attack by the reactive thiol group on the imine bond to form a stable fused product, **9** shown in Fig. 4a. The condensation between aminothiols and aldehydes to form thiazolidines is an interesting bioorthogonal reaction[64–66] given that the aminothiol group exists naturally in proteins. Conventionally, thiazolidine ring formation is reversible and requires long reaction times (up to several days) and high concentrations of reactants.[65,66] Here, the reaction was carried out in ambient microdroplets between cysteamine, **6** and 2-FPBA, and the corresponding mass spectrum shows the presence of thiazolidinoboronate product, $[\mathbf{9+H}]^+$ at *m*/*z* 210 as well as unreacted cysteamine, $[\mathbf{6+H}]^+$ at *m*/*z* 78, respectively. The MS/MS spectrum shows successive losses of water (Fig. 4c), and this, together with a comparison between the calculated isotopic distribution and experimental mass spectra (Fig. S9†), confirms the reaction product as thiazolidinoboronate, **9**. The highly reactive thiol group favours the reaction and leads to oxidative dimerization of cysteamine, **6** to form cystamine, **7**.

Diazaborine complex formation in microdroplets

Diazaborine formation is an important reaction that utilizes hydrazine to generate an iminoboronate. This compound class finds applications in enzyme inhibition,[67] as well as for its antibacterial properties.[47,59] The bulk solution reaction between phenylhydrazine and 2-FPBA is known to occur rapidly to give diazaborine heterocycles with rate constants $\sim 10^3\ M^{-1}\ s^{-1}$.[68,69] Previous reports suggest that the stereochemical arrangement of the α-nucleophile (phenylhydrazine) and *ortho*-carbonyl phenylboronic acid controls the formation and stability of diazaborine.[70] The reaction relies on the facile ring closure from the hydrazone. Here, microdroplet-assisted diazaborine formation can proceed *via* the formation of either isomeric hydrazone (**11** or **13**) in the first step (Fig. 5a), depending on which N atom is involved in imine formation. This intermediate product pair is observed as the Na^+ adduct at *m*/*z* 263. In the second step, ring closure occurs to eliminate water and form one or other isomer of the corresponding protonated diazaborine, observed at *m*/*z* 223 (Fig. 5b). The MS/MS spectrum of the diazaborine (Fig. 5c) shows fragment peaks that strongly suggest contributions from both isomeric precursor ions:

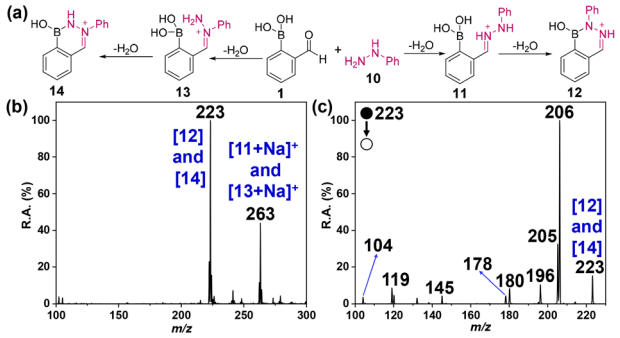

Fig. 5 (a) Formation of diazaborine *via* iminoboronate in electrosprayed microdroplets. (b) Positive mode nESI mass spectrum of the products of reaction between phenylhydrazine and 2-FPBA in ACN microdroplets. Labeling connects the main peaks with isomeric structures. (c) MS/MS spectrum of the mass-selected diazaborine product, **12** or **14**, *m/z* 223, recorded using collision-induced dissociation (CID).

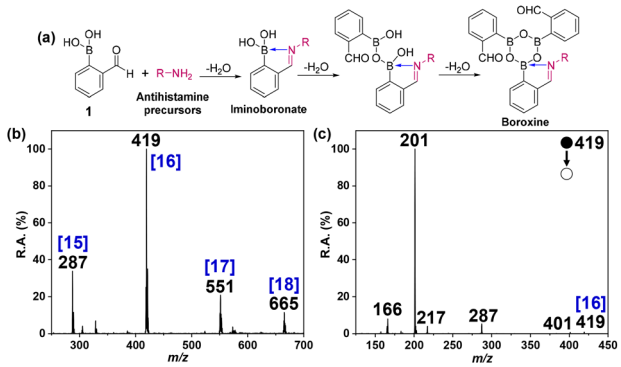

Fig. 6 (a) Late-stage functionalization of antihistamine precursors using iminoboronate chemistry in electropsrayed microdroplets. (b) Positive mode mass spectrum of the products of the reaction between nor-cetirizine and 2-FPBA in ACN microdroplets. (c) MS/MS spectrum of the mass-selected protonated boroxine, **16** (*m/z* 419), recorded using CID. MS/MS spectra of other products are provided in the ESI.†

notably the main fragment due to the loss of hydroxyl is assigned to **12** as a precursor, while the isomer **14** is most reasonably associated with the loss of water and HOBNH according to the fragmentation mechanisms provided in Fig. S10.† In addition, there is good agreement between the expected and measured isotope distributions (Fig. S11†). The peak at 27.66 ppm in the ^{11}B NMR spectrum (Fig. S12†) is a characteristic signature of the diazaborine product, **12** or **14**, as observed in a previous report.[61]

Late-stage functionalization (LSF) based on click chemistry using boronic acids

Accelerated chemical reactions in microdroplets can be utilized as a method of LSF, an alternative to traditional *de novo* synthesis.[71–73] This is an effective tool to rapidly explore chemical space, a key step in drug discovery.[12,13] Here, we demonstrate the utilization of iminoboronate chemistry by targeting the cyclic secondary amine center present in several antihistamine precursors. First-generation antihistamines are known to cross the blood–brain barrier (BBB) and cause unwanted interference such as sedation, drowsiness, fatigue, reduced sleep, and impaired concentration.[74] The BBB penetration is related to the lipophilicity, size, structure, molecular weight, and charge of antihistamines. Specifically, lipophilicity facilitates BBB penetration, whereas the charged interaction and higher molecular weight (typically >400–600 Da) hinder BBB penetration.[74,75]

Here, accelerated click chemistry was applied to access modified antihistamines with high molecular weights and a permanent charge using the reaction of secondary amines to form charged imines. The reaction proceeds to give the corresponding iminoboronate and the boroxine products (Fig. 6a). Note that this boroxine is structurally different from **4**, obtained by the reaction with butylamine (Fig. 1). Antihistamine precursors are sterically crowded due to the presence of bulky phenyl groups and their cyclic secondary amines; they do not lead to additional iminoboronate formation. The iminoboronate-based LSF was successfully applied to functionalize six different antihistamine precursors (Scheme 2a). The complex drug molecules were functionalized at the desired site under ambient conditions without using a catalyst. This successful result shows the potential application of this type of microdroplet-accelerated reaction in LSF for the creation of modified drugs. The mass spectrum recorded for the reaction product of a representative antihistamine precursor, norcetirizine, and 2-FPBA (Fig. 6b) shows unreacted norcetirizine, **[15]**, the protonated iminoboronate product, **[16]**, an additional dehydration product, **[17]**, and the desired boroxine, **[18]**. Intermolecular condensation between iminoboronate and 2-FPBA gives the dimer at *m/z* 551. The structures of all these products are shown in Scheme 2b. Structural confirmation of the iminoboronate product, **16** was derived from MS/MS (Fig. 6c) and by comparing the isotopic distributions between the calculated isotopic distribution and experimental data (Fig. S13†). Structures of all the fragment peaks observed in

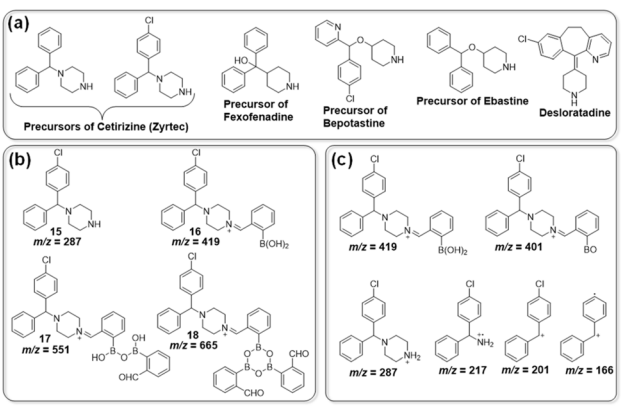

Scheme 2 (a) Structures of the antihistamine precursors used for the imnoboronate-based LSF. (b) Structures of the observed ions as noted in Fig. 4b. (c) Fragment ion structures observed in the MS/MS spectrum shown in Fig. 5c.

Fig. 6c are suggested in Scheme 2c. MS/MS spectra and isotopic distribution comparison of other products (**17** and **18**) are provided in Fig. S14–S17.† The mass spectra corresponding to the LSF reaction of other antihistamine precursors with 2-FPBA are also shown (Fig. S18–S22†).

Reaction time scale, conversion ratio (yield), and the mechanism

In this work, all the chemical reactions occur during the flight of nESI-generated microdroplets, which is estimated to take time in the low millisecond range (droplet velocity 6 m s^{-1}; flight distance 10 mm) as noted in previous studies.[76,77] Considering that the fastest of these reactions on the bulk scale takes time on the minute scale,[43,68,69] the microdroplet reactions in this format are three to four orders of magnitude faster. This estimate is consistent with many earlier estimates of reaction rate acceleration in microdroplet experiments.[23,78–81] Apart from reaction rates, interest focuses on the yields and scale of these microdroplet reactions. The degree to which a microdroplet reaction occurs can be monitored using the conversion ratio (CR), a measurement of the ratio of ion intensities of the product, [P] relative to the sum of the product and starting material ion intensities, ([P]/[SM] + [P]).[13,78] The CR is a surrogate for yield, which is not directly measurable in femtoliter-scale reaction vessels. For reactions like those studied here, in which ionic reactants give ionic products of similar proton affinity, CR is a good measure of yield.[13,78] Table 1 shows the CR values for some of the microdroplet reactions studied. The values are generally high and by-products are noted in the mass spectra, for example, those formed by further condensation involving the main iminoboronate products (Fig. S18–S22†). In the case of Fig. 4a, the low CR is due to the dimerization of cysteamine in a side reaction. Although these products were formed in the milligram scale, it is important to note that scale-up is straightforward, as described in the literature and illustrated for this system in ESI,† Section 1.6.

Addressing the mechanism, all the reactions appear to follow an acid-catalysed condensation pathway, for which there are many precedents amongst microdroplet reactions.[1,21,31,82–88] It is generally accepted that these reactions are driven by the superacidic interface of microdroplets.[28,29] This superacidity protonates 2-FPBA to create the charged species in the first step (see ESI,† Section 1.5), with subsequent facile dehydration of the 'dry' (water-scarce) microdroplet interface. This superacid-catalysed condensation mechanism is followed for all the reactions presented and is suggested to be the basis for the observed reaction acceleration. It is also significant that the entire sequence of reactions (multiple dehydration steps) occurs in the individual microdroplets.

Table 1 Conversion ratio (CR) for reactions in microdroplets between amines and 2-formyl phenylboronic acid (2-FPBA)

Amines	CR (%)	Amines	CR (%)
Butylamine (Fig. 1a)	100[a]	Antihistamine (Fig. S19)	53
Phenylhydrazine (Fig. 5a)	100[a]	Antihistamine (Fig. S20)	34
Cysteamine (Fig. 4a)	57	Antihistamine (Fig. S21)	81
Antihistamine (Fig. 6a)	75	Antihistamine (Fig. S22)	75
Antihistamine (Fig. S18)	54		

[a] CRs for Fig. 1a and 5a were estimated to be 100% due to the complete conversion as the peaks corresponding to the starting materials (amine) were not observed.

Conclusions

We demonstrate the first example of accelerated click reactions based on dehydration that occur in microdroplets, occurring under ambient conditions without a catalyst. The reaction leads to the formation of different product types (iminoboronate, boroxine, thiazolidine, and diazaborine) depending on the chosen amines, as confirmed by tandem mass spectrometry and NMR. These reactions, like many others now being encountered in microdroplet chemistry, are favoured by two properties of the air–liquid interface: namely, its superacidity and its intrinsically dry nature, which together circumvent the need for expensive catalysts, high temperatures, and long reaction times. Furthermore, these click reactions can be utilized as an efficient LSF tool to access a range of modified antihistamine drugs under ambient conditions. This illustrates the versatility and chemical scope of the reaction, which should be amenable to reaction screening in drug discovery and also as an efficient synthetic tool.

Data availability

All data on which this publication is based appear either in the main text or in the ESI.† The underlying raw data are available on request to the authors.

Author contributions

Dr R. G. Cooks and Dr J. Ghosh designed the experiments. Dr J. Ghosh performed the experiments. Dr R. G. Cooks and Dr J. Ghosh analyzed the results and wrote the manuscript.

Conflicts of interest

There are no conflicts to declare.

Acknowledgements

The authors acknowledge financial support from the National Center for Advancing Translational Sciences (NCATS) through the ASPIRE (A Specialized Platform for Innovative Research Exploration) Reduction-to-Practice Challenge and Collaborative Research Program (UG3/UH3 TR004139) as well as from the Multi-University Research Initiative (MURI) of the Air Force Office of Scientific Research (FA9550-21-1-0170) *via* Stanford University (subaward 62741613-204669). We also acknowledge Prof. T. Pradeep, IIT Madras, for his interest in the context of the Purdue-India Partnership.

References

1 M. Girod, E. Moyano, D. I. Campbell and R. G. Cooks, *Chem. Sci.*, 2011, **2**, 501–510.
2 S. Banerjee and R. N. Zare, *Angew. Chem.*, 2015, **127**, 15008–15012.
3 D. Kuai, H. Cheng, K.-Y. Kuan and X. Yan, *Chem. Commun.*, 2021, **57**, 3757–3760.
4 B. Zheng, X. Jin, J. Liu and H. Cheng, *ACS Sustain. Chem. Eng.*, 2021, **9**, 4383–4390.
5 L. Xue, B. Zheng, J. Sun, J. Liu and H. Cheng, *ACS Sustain. Chem. Eng.*, 2023, **11**, 12780–12789.
6 Y. Wu, H. Cheng, J. Li, J. Liu and J. Sun, *J. Org. Chem.*, 2023, **88**, 11186–11196.
7 J. Ghosh and R. G. Cooks, *TrAC, Trends Anal. Chem.*, 2023, **161**, 117010.
8 J. Ghosh and R. G. Cooks, *ChemPlusChem*, 2022, **87**, e202200252.
9 A. Jana, S. K. Jana, D. Sarkar, T. Ahuja, P. Basuri, B. Mondal, S. Bose, J. Ghosh and T. Pradeep, *J. Mater. Chem. A*, 2019, **7**, 6387–6394.
10 J. K. Lee, D. Samanta, H. G. Nam and R. N. Zare, *Nat. Commun.*, 2018, **9**, 1562.
11 H. Fang, K. Huang, L. Yuan, X. Wu, D. Wang, H. Chen and S. Feng, *New J. Chem.*, 2016, **40**, 7294–7298.
12 K.-H. Huang, N. M. Morato, Y. Feng and R. G. Cooks, *Angew. Chem., Int. Ed.*, 2023, **62**, e202300956.
13 K.-H. Huang, N. M. Morato, Y. Feng, A. Toney and R. G. Cooks, *J. Am. Chem. Soc.*, 2024, **146**, 33112–33120.
14 J. Ghosh, N. M. Morato, Y. Feng and R. G. Cooks, *ChemPlusChem*, 2025, e202500164.
15 D. Zhang, J. Wang, H. Chen, C. Gong, D. Xing, Z. Liu, I. Gladich, J. S. Francisco and X. Zhang, *J. Am. Chem. Soc.*, 2023, **145**, 6462–6470.
16 Z. Wan, C. Zhu and J. S. Francisco, *J. Am. Chem. Soc.*, 2023, **145**, 17478–17484.
17 M. Kumar, J. Zhong, X. C. Zeng and J. S. Francisco, *J. Am. Chem. Soc.*, 2018, **140**, 4913–4921.
18 X. Zhang, R. Su, J. Li, L. Huang, W. Yang, K. Chingin, R. Balabin, J. Wang, X. Zhang, W. Zhu, K. Huang, S. Feng and H. Chen, *Nat. Commun.*, 2024, **15**, 1535.
19 D. T. Holden, N. M. Morato and R. G. Cooks, *Proc. Natl. Acad. Sci. U. S. A.*, 2022, **119**, e2212642119.
20 L. Qiu and R. G. Cooks, *Proc. Natl. Acad. Sci. U. S. A.*, 2024, **121**, e2309360120.
21 I. Nam, J. K. Lee, H. G. Nam and R. N. Zare, *Proc. Natl. Acad. Sci. U. S. A.*, 2017, **114**, 12396–12400.
22 L. Qiu, Z. Wei, H. Nie and R. G. Cooks, *ChemPlusChem*, 2021, **86**, 1362–1365.
23 X. Yan, R. M. Bain and R. G. Cooks, *Angew. Chem., Int. Ed.*, 2016, **55**, 12960–12972.
24 J. K. Lee, K. L. Walker, H. S. Han, J. Kang, F. B. Prinz, R. M. Waymouth, H. G. Nam and R. N. Zare, *Proc. Natl. Acad. Sci. U. S. A.*, 2019, **116**, 19294–19298.
25 J. K. Lee, D. Samanta, H. G. Nam and R. N. Zare, *J. Am. Chem. Soc.*, 2019, **141**, 10585–10589.
26 D. Gao, F. Jin, J. K. Lee and R. N. Zare, *Chem. Sci.*, 2019, **10**, 10974–10978.
27 X. Zhang, K. Huang, Y. Fu, N. Zhang, X. Kong, Y. Cheng, M. Zheng, Y. Cheng, T. Zhu, B. Fu, S. Feng and H. Chen, *Nat. Commun.*, 2024, **15**, 5881.
28 K.-H. Huang, Z. Wei and R. G. Cooks, *Chem. Sci.*, 2021, **12**, 2242–2250.
29 J. Ghosh, J. Mendoza and R. G. Cooks, *Angew. Chem., Int. Ed.*, 2022, **61**, e202214090.
30 A. Fallah-Araghi, K. Meguellati, J.-C. Baret, A. E. Harrak, T. Mangeat, M. Karplus, S. Ladame, C. M. Marques and A. D. Griffiths, *Phys. Rev. Lett.*, 2014, **112**, 028301.
31 N. Sahota, D. I. AbuSalim, M. L. Wang, C. J. Brown, Z. Zhang, T. J. El-Baba, S. P. Cook and D. E. Clemmer, *Chem. Sci.*, 2019, **10**, 4822–4827.
32 N. Narendra, X. Chen, J. Wang, J. Charles, R. G. Cooks and T. Kubis, *J. Phys. Chem. A*, 2020, **124**, 4984–4989.
33 Z. Zhou, X. Yan, Y.-H. Lai and R. N. Zare, *J. Phys. Chem. Lett.*, 2018, **9**, 2928–2932.
34 X. Zhong, H. Chen and R. N. Zare, *Nat. Commun.*, 2020, **11**, 1049.
35 K. Luo, J. Li, Y. Cao, C. Liu, J. Ge, H. Chen and R. N. Zare, *Chem. Sci.*, 2020, **11**, 2558–2565.
36 J. Li, C. Liu, H. Chen and R. N. Zare, *J. Org. Chem.*, 2021, **86**, 5011–5015.
37 P. Zhao, H. P. Gunawardena, X. Zhong, R. N. Zare and H. Chen, *Anal. Chem.*, 2021, **93**, 3997–4005.
38 H. P. Gunawardena, Y. Ai, J. Gao, R. N. Zare and H. Chen, *Anal. Chem.*, 2023, **95**, 3340–3348.
39 X. Zhang, P. Hu, M. Duan, K. Chingin, R. Balabin, X. Zhang and H. Chen, *Chem. Sci.*, 2024, **15**, 16125–16132.
40 X. Li, Y. Zhang, Z. Shi, D. Wang, H. Yang, Y. Zhang, H. Qin, W. Lu, J. Chen, Y. Li and G. Qing, *Nat. Commun.*, 2024, **15**, 1207.
41 S. Chatterjee, E. V. Anslyn and A. Bandyopadhyay, *Chem. Sci.*, 2021, **12**, 1585–1599.
42 S. Delpierre, B. Willocq, J. De Winter, P. Dubois, P. Gerbaux and J.-M. Raquez, *Chem.–Eur. J.*, 2017, **23**, 6730–6735.
43 H. Faustino, M. J. S. A. Silva, L. F. Veiros, G. J. L. Bernardes and P. M. P. Gois, *Chem. Sci.*, 2016, **7**, 5052–5058.
44 P. M. S. D. Cal, J. B. Vicente, E. Pires, A. V. Coelho, L. F. Veiros, C. Cordeiro and P. M. P. Gois, *J. Am. Chem. Soc.*, 2012, **134**, 10299–10305.
45 Y. Pérez-Fuertes, A. M. Kelly, A. L. Johnson, S. Arimori, S. D. Bull and T. D. James, *Org. Lett.*, 2006, **8**, 609–612.
46 S. Delpierre, B. Willocq, G. Manini, V. Lemaur, J. Goole, P. Gerbaux, J. Cornil, P. Dubois and J.-M. Raquez, *Chem. Mater.*, 2019, **31**, 3736–3744.
47 G. Kocak, H. Cicek, Ö. Ceylan and V. Bütün, *J. Appl. Polym. Sci.*, 2019, **136**, 46907.
48 R. S. Scott, A. J. Veinot, D. L. Stack, P. T. Gormley, B. N. Khuong, C. M. Vogels, J. D. Masuda, F. J. Baerlocher, T. J. MacCormack and S. A. Westcott, *Can. J. Chem.*, 2018, **96**, 906–911.
49 A. P. Côté, A. I. Benin, N. W. Ockwig, M. O'Keeffe, A. J. Matzger and O. M. Yaghi, *Science*, 2005, **310**, 1166–1170.

50 H. M. El-Kaderi, J. R. Hunt, J. L. Mendoza-Cortés, A. P. Côté, R. E. Taylor, M. O'Keeffe and O. M. Yaghi, *Science*, 2007, **316**, 268–272.
51 E. Hamzehpoor, F. Effaty, T. H. Borchers, R. S. Stein, A. Wahrhaftig-Lewis, X. Ottenwaelder, T. Friščić and D. F. Perepichka, *Angew. Chem., Int. Ed.*, 2024, e202404539.
52 K. Wu and A. G. Doyle, *Nat. Chem.*, 2017, **9**, 779–784.
53 Z. T. Ariki, Y. Maekawa, M. Nambo and C. M. Crudden, *J. Am. Chem. Soc.*, 2018, **140**, 78–81.
54 K. Ono and N. Iwasawa, *J. Inclusion Phenom. Macrocyclic Chem.*, 2021, **101**, 19–29.
55 G. Alcaraz, L. Euzenat, O. Mongin, C. Katan, I. Ledoux, J. Zyss, M. Blanchard-Desce and M. Vaultier, *Chem. Commun.*, 2003, 2766–2767.
56 H. Konishi, T. Minato, T. Abe and Z. Ogumi, *Chem. Lett.*, 2018, **47**, 1346–1349.
57 A. Bandyopadhyay, S. Cambray and J. Gao, *Chem. Sci.*, 2016, **7**, 4589–4593.
58 A. Bandyopadhyay, S. Cambray and J. Gao, *J. Am. Chem. Soc.*, 2017, **139**, 871–878.
59 G. Högenauer and M. Woisetschläger, *Nature*, 1981, **293**, 662–664.
60 A. L. Korich and P. M. Iovine, *Dalton Trans.*, 2010, **39**, 1423–1431.
61 A. L. Dey, *Molecules*, 2024, **29**, 4998.
62 A. Térol, G. Subra, J. P. Fernandez, Y. Robbe, J. P. Chapat and R. Granger, *Org. Magn. Reson.*, 1981, **17**, 68–70.
63 D. Bermejo-Velasco, G. N. Nawale, O. P. Oommen, J. Hilborn and O. P. Varghese, *Chem. Commun.*, 2018, **54**, 12507–12510.
64 X. Bi, K. K. Pasunooti, A. H. Tareq, J. Takyi-Williams and C.-F. Liu, *Org. Biomol. Chem.*, 2016, **14**, 5282–5285.
65 X. Liu, Y. Wang, B. Ye and X. Bi, *Chem. Sci.*, 2023, **14**, 7334–7345.
66 A. Chowdhury, S. Chatterjee, A. Kushwaha, S. Nanda, T. J. Dhilip Kumar and A. Bandyopadhyay, *Chem.–Eur. J.*, 2023, **29**, e202300393.
67 M. J. S. Dewar and R. C. Dougherty, *J. Am. Chem. Soc.*, 1962, **84**, 2648–2649.
68 C. J. Stress, P. J. Schmidt and D. G. Gillingham, *Org. Biomol. Chem.*, 2016, **14**, 5529–5533.
69 H. Gu, S. Ghosh, R. J. Staples and S. L. Bane, *Bioconjugate Chem.*, 2019, **30**, 2604–2613.
70 D. F. Nippa, K. Atz, R. Hohler, A. T. Müller, A. Marx, C. Bartelmus, G. Wuitschik, I. Marzuoli, V. Jost, J. Wolfard, M. Binder, A. F. Stepan, D. B. Konrad, U. Grether, R. E. Martin and G. Schneider, *Nat. Chem.*, 2024, **16**, 239–248.
71 L. Guillemard, N. Kaplaneris, L. Ackermann and M. J. Johansson, *Nat. Rev. Chem*, 2021, **5**, 522–545.
72 N. J. Castellino, A. P. Montgomery, J. J. Danon and M. Kassiou, *Chem. Rev.*, 2023, **123**, 8127–8153.
73 K.-H. Huang, J. Ghosh, S. Xu and R. G. Cooks, *ChemPlusChem*, 2022, **87**, e202100449.
74 P. Das, M. D. Delost, M. H. Qureshi, D. T. Smith and J. T. Njardarson, *J. Med. Chem.*, 2019, **62**, 4265–4311.
75 W. A. Banks, *BMC Neurol.*, 2009, **9**, S3.
76 R. M. Bain, C. J. Pulliam, S. T. Ayrton, K. Bain and R. G. Cooks, *Rapid Commun. Mass Spectrom.*, 2016, **30**, 1875–1878.
77 R. D. Espy, A. R. Muliadi, Z. Ouyang and R. G. Cooks, *Int. J. Mass Spectrom.*, 2012, **325–327**, 167–171.
78 Z. Wei, Y. Li, R. G. Cooks and X. Yan, *Annu. Rev. Phys. Chem.*, 2020, **71**, 31–51.
79 P. Kim, R. S. Reynolds, A. M. Deal, V. Vaida, M. Ahmed and K. R. Wilson, *J. Phys. Chem. Lett.*, 2024, **15**, 11131–11138.
80 C. J. Chen and E. R. Williams, *Chem. Sci.*, 2023, **14**, 4704–4713.
81 K. R. Wilson and A. M. Prophet, *Annu. Rev. Phys. Chem.*, 2024, **75**, 185–208.
82 M. Li, C. Boothby, R. E. Continetti and V. H. Grassian, *J. Am. Chem. Soc.*, 2023, **145**, 22317–22321.
83 M. Li, S. Yang, M. Rathi, S. Kumar, C. S. Dutcher and V. H. Grassian, *Chem. Sci.*, 2024, **15**, 13429–13441.
84 R. M. Bain, C. J. Pulliam and R. G. Cooks, *Chem. Sci.*, 2014, **6**, 397–401.
85 J. Li, J. Sun, Y. Wang, J. Liu and H. Cheng, *ACS Sustain. Chem. Eng.*, 2025, **13**, 571–582.
86 C. Dai, C. Huang, M. Ye, J. Liu and H. Cheng, *J. Org. Chem.*, 2024, **89**, 14818–14830.
87 X. Jin, Y. Wu, J. Sun, J. Liu and H. Cheng, *Analysis Sensing*, 2023, **3**, e202300031.
88 X. Jin, Y. Wu, C. Dai, J. Sun, M. Ye, J. Liu and H. Cheng, *ChemPlusChem*, 2023, **88**, e202200206.